J. Fluid Mech. (2025), *vol*. 1002, A7, doi:10.1017/jfm.2024.1112

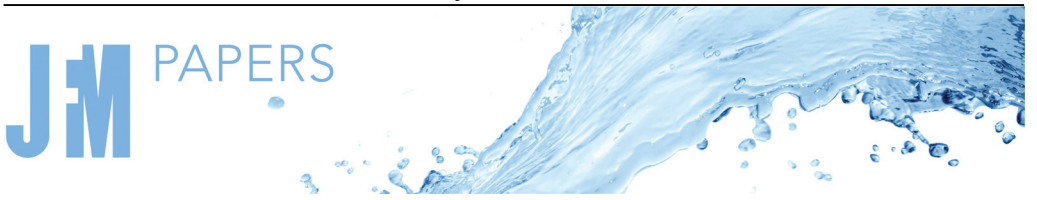

The impact of natural convection and turbulent mixing on mechanical ventilation

Daniel A. Toy[1] **and Andrew W. Woods**[1],†

[1]Institute for Energy and Environmental Flows, University of Cambridge, Madingley Road, Cambridge CB3 0EZ, UK

(Received 23 April 2024; revised 16 October 2024; accepted 29 October 2024)

We explore the interaction of natural convection and mechanical ventilation in a room where fresh air is supplied at low level and stale air is extracted at high level. Turbulent buoyant plumes rising from heat sources interact with this upward airflow and establish a steady-state stratification with a warm upper layer above a layer of the cold supply air. Adapting the volume balance model used in natural ventilation (Linden *et al.*, *J. Fluid Mech.*, vol. 212, 1990, pp. 309–335) leads to the prediction that the upper layer will vent from the room when the ventilation volume flux exceeds the volume flux in the plumes at the ceiling. However, our new laboratory experiments establish that there is still a stable two-layer stratification beyond this point of critical ventilation. Motivated by our observations, we propose that the kinetic energy flux supplied by the plume leads to turbulent mixing in the upper layer. We propose a new model of this mixing which is consistent with our experiments in both the over- and under-ventilated regimes. This has important implications for air recirculation in buildings with large ventilation flows, particularly hospital operating theatres and clean rooms.

Key words: convection in cavities, plumes/thermals

1. Introduction

The air quality in the built environment is intricately linked to our comfort, health and productivity. As a result, ventilation is a necessity in all types of buildings, from offices and auditoriums to factories and operating theatres, supplying fresh air and removing contaminants. In one arrangement, called underfloor air distribution, fresh air is supplied through an underfloor plenum to low-level vents, and stale air is extracted through high-level vents. The resulting upward displacement flow then interacts with turbulent

† Email address for correspondence: andy@bpi.cam.ac.uk

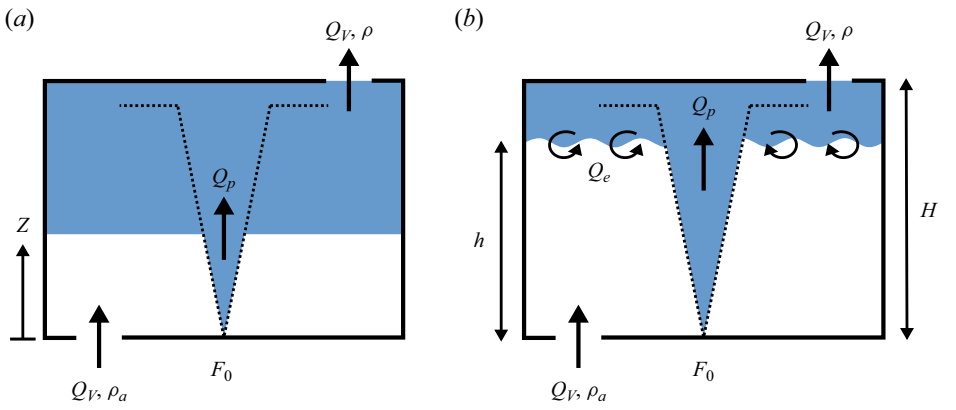

Figure 1. Schematic of the steady-state stratification (*a*) in the under-ventilated regime where the interface is sharp and only crossed by fluid in the plume and (*b*) in the over-ventilated regime where a significant flux of fluid is entrained from the lower layer into the upper layer, which then mixes with fluid from the plume.

buoyant plumes rising from heat sources, including people and electrical equipment, leading to thermal stratification. This establishes a steady state with a warmer upper layer above a layer of the cold supply air. The interface depth between these layers depends on a dynamic equilibrium between the ventilation flow, which raises the interface, and the plume, which works to lower the interface. This is shown schematically in figure 1.

With well-designed ventilation, the interface is above the occupied zone, the occupants are surrounded by fresh air and heat and contaminants are transported into the upper layer before extraction. This leads to improved thermal comfort, and the air the occupant breathes will have a lower concentration of contaminants compared with mixing ventilation schemes.

Models for ventilation have evolved over the last several decades, drawing from work on turbulent buoyant plumes mixing in a confined space (Baines & Turner 1969; Linden, Lane-Serff & Smeed 1990). In their work on natural ventilation, Linden *et al.* (1990) proposed a volume balance model, where the net upward volume flux through any horizontal cross-section is equal to the ventilation volume flux. If there is a depth, h, at which the plume volume flux matches the ventilation volume flux, this model would suggest that vertical velocity in the fluid outside the plume is zero and an interface forms between the upper and lower layers. To estimate the depth of this interface, we introduce a model for the volume flux in a plume. For a pure plume rising through a uniform environment from a source of buoyancy flux, πF_0, Morton, Taylor & Turner (1956) showed that the specific volume flux, πQ_p, a distance z above the source is

$$Q_p(z) = \lambda F_0^{1/3} z^{5/3}, \tag{1.1}$$

Here, λ is an empirical constant related to entrainment into the plume (see § 3.1). In a mechanically ventilated system with total ventilation volume flux, πQ_V, then at the depth of the interface, h,

$$Q_V = \lambda F_0^{1/3} h^{5/3}. \tag{1.2}$$

If we scale the depth of the interface, h, by the total height of the room, H, giving $\xi = h/H$, and introduce the dimensionless parameter

$$\mu = \frac{\lambda F_0^{1/3} H^{5/3}}{Q_V}, \tag{1.3}$$

which represents the ratio of the volume flux in a pure plume at height H to the ventilation volume flux, then we find that

$$\xi = \mu^{-3/5}. \tag{1.4}$$

This suggests that the interface depth, ξ, only depends on the dimensionless parameter μ and is independent of the cross-sectional area of the room. Provided that $\mu > 1$, then $\xi < 1$. We refer to this as the under-ventilated regime. Decreasing the volume flux in the plume or increasing the ventilation rate will decrease the value of μ and, from (1.4), this volume balance model predicts that, when $\mu = 1$, the interface reaches the top of the room. We call this critical ventilation. The model breaks down for $0 < \mu < 1$ because it predicts that the interface is above the ceiling. This over-ventilated regime arises when the total ventilation volume flux exceeds the volume flux in the plume at the ceiling.

Because (1.4) breaks down for $\mu < 1$, we have conducted new laboratory experiments to explore the transition from the under-ventilated ($\mu > 1$) to the over-ventilated ($\mu < 1$) regime. These new experiments establish that there is, in fact, still a stable two-layer stratification in the over-ventilated regime and that the volume balance model significantly overpredicts the measured interface depths above the base of the room when the flow is close to critical ventilation ($\mu \approx 1$). Our observations suggest that turbulent mixing in the upper layer associated with the kinetic energy flux supplied by the plume entrains fluid from the lower layer into the upper layer. We propose a new model for this mixing, which is consistent with the interface height in our experiments across both regimes.

The structure of this paper is as follows. In § 2, we describe our new laboratory experiments and observations for the over- and under-ventilated regimes. We propose a new model for the mixing in § 3 and compare the theoretical predictions of this model with our experiments in § 4. We apply this model to natural ventilation in § 5. We examine the implications for the design of ventilation systems in § 6 and draw some conclusions in § 7.

2. Experimental model of over- and under-ventilation

We performed a series of systematic laboratory experiments to investigate the flow structure and density stratification in both over- and under-ventilated regimes. We describe the experimental apparatus and then present qualitative results. These observations are then used in § 3 to inform model development.

2.1. *Experimental method*

For ease, the experiments were performed in an inverted geometry with a dense descending saline plume modelling a real heat source. Due to the small magnitude of the density differences, the Boussinesq approximation is valid and inverting the geometry has no significant impact on the dynamics of the experiment.

An open-topped tank, with internal dimensions 0.25 by 0.25 by 0.30 m or 0.75 by 0.75 by 0.50 m, was submerged in a larger tank that acted as a reservoir of fresh water. Fluid was withdrawn through pipes at the base of the smaller tank using a peristaltic pump, while the open top allowed for a uniform inflow.

A plume was created by supplying a dense salt solution to a nozzle designed to produce a turbulent plume with a relatively small source volume and momentum flux. The room height, H, was taken to be the distance from the source to the base of the tank plus the distance from the source to the virtual origin, z_0, of the plume (see § 3). Throughout the

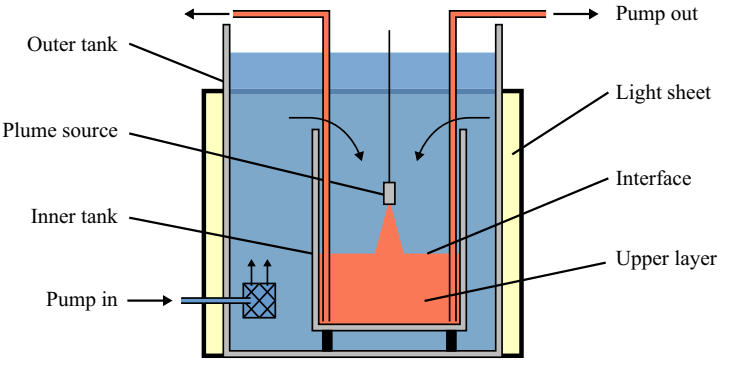

Figure 2. Schematic illustrating the experimental set-up. A small open-topped tank is submerged in a larger tank of fresh water. Fluid is withdrawn from the base of the tank through multiple openings using a pump, while the open top allows for uniform inflow. A suspended plume source is supplied with a dense saltwater solution that has been dyed red, and a two-layer stratification is established and photographed using a DSLR camera placed approximately 5 m from the tank.

experiment, the outer tank of fresh water was refilled using a third peristaltic pump so that the depth of water above the model room remained constant.

The flow was examined using a dye attenuation technique. A light sheet was placed behind the tank to provide uniform illumination, red dye was added to the plume fluid and the experiment was recorded using a DSLR camera. This is shown schematically in figure 2. To minimise the parallax error, the camera was positioned far back from the tank ($\gtrsim$5 m) and focused on the centre of the model room close to the interface. This means the line-of-sight average dye concentration will be close to the horizontal depth-averaged concentration.

The principle of the dye attenuation technique is that light passing through the tank will be partially absorbed by regions of dyed fluid, which changes the pixel intensity measured by the sensor in the camera. When dyed fluid mixes with clear fluid, the dye is diluted and will absorb less light. We can convert the measured pixel intensity to the line-of-sight average dye concentration using a set of empirical calibration curves. Then, assuming that the same processes mix dye and salt, the density distribution in the tank can be calculated.

Before the main experiments, we produced calibration curves for the particular combination of camera settings, tanks, dyes and light sheets. The outer tank was filled with fresh water, and the inner tank was filled with a known dye concentration. The pixel intensity was measured, and this process was repeated for a range of dye concentrations. In the present experiments, we used the blue channel, which had the largest change in pixel intensity as the dye concentration increased and, therefore, minimised any error. Furthermore, care was taken to ensure the highest concentration was within the approximately linear portion of the curve relating dye concentration to pixel intensity to avoid issues related to signal saturation.

A typical experiment consisted of the following steps: first, we prepared the plume fluid by adding salt and dye to fresh water. Next, all three peristaltic pumps were turned on and balanced to avoid net accumulation or loss of fluid in the experimental tanks. The system was then run for a sufficiently long time to reach a steady state and examined using the light attenuation technique.

Before presenting the results, we note that it is possible for the extraction rate through the outflow pipes to be so large that the upper layer of fresh water is drawn directly down to the

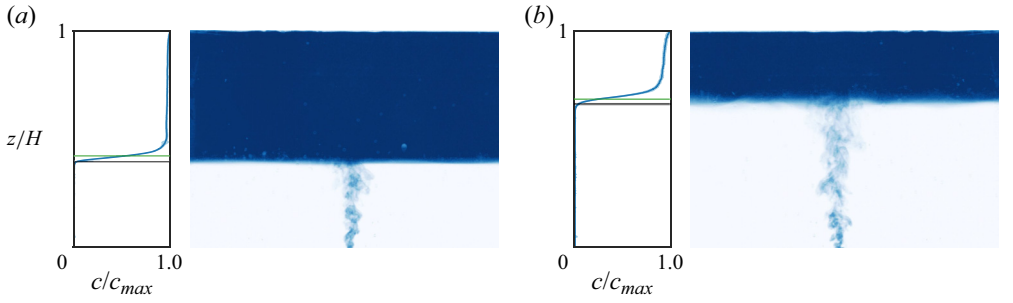

Figure 3. Typical experimental results for the under-ventilated regime showing the horizontally averaged dye concentration of five experiments and a false colour image showing the instantaneous dye distribution in the tank for (*a*) $\mu = 3.41$ and (*b*) $\mu = 1.75$. The black horizontal line shows the measured interface depth, and the grey shaded region indicates the variation in the measurement. The green horizontal line shows the interface depth predicted by the volume balance model.

outflow, bypassing the lower layer of saline fluid. However, in the present experiments, the flow rates were chosen to avoid this phenomenon. This is discussed further in Appendix B.

2.2. *Experimental observations*

In the remainder of the paper, for convenience, we present the experimental results rotated by 180° so that they correspond to the schematic diagram of a building ventilation system (figure 1). As such, the text refers to an ascending plume and a mixed layer at the top of the ventilated space.

Figures 3–5 illustrate typical experimental results. In these experiments, the height of the tank, H, and buoyancy flux, πF_0, from the plume source were fixed, while the ventilation volume flux, πQ_V, was adjusted so that the ratio of the volume flux in the plume to the ventilation volume flux, μ, varied between 3.41 and 0.34. This allowed us to investigate the flow and density stratification in the under-ventilated regime ($\mu > 1$) through critical ventilation ($\mu = 1$) and into the over-ventilated regime ($\mu < 1$).

The left-hand plot in every pair of figures shows the average vertical concentration profile (solid line) and standard deviation (shaded region) of five experiments at the same value of μ. The profile has been rescaled using the maximum concentration, which is the concentration extracted by the ventilation. This profile is obtained by excluding the centre of the frame so that the plume does not obstruct the measurement of the surrounding stratification. The black horizontal lines show the interface depth obtained by a thresholding routine (see Appendix A). The solid line is the time-averaged interface location, and the grey-shaded region indicates the variation in the measured depth. In the under-ventilated regime, before the volume balance model breaks down, (1.4) is used to predict the interface depth. This prediction is plotted with a green horizontal line. The right-hand figure in each pair is a snapshot of the steady state converted into a false colour image. A consistent colour scale was applied across the images.

In all of the steady states, the system establishes a two-layer stratification: an upper layer with a high dye concentration and a lower layer with zero concentration. We observe that as the ratio of the volume fluxes, μ, decreases, the interface between the layers rises. Qualitatively, this is consistent with the volumetric model presented in § 1. However, based on that model, we would expect the interface to reach the top of the room between figures 4(*a*) and 4(*b*) when the system passes critical ventilation. This is not the case.

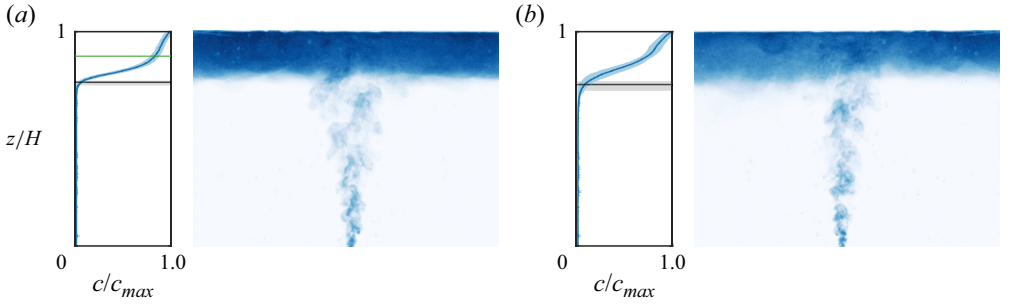

Figure 4. Typical experimental results spanning the critically ventilated regime showing the horizontally averaged dye concentration of five experiments and a false colour image showing the instantaneous dye distribution in the tank for (*a*) $\mu = 1.20$ and (*b*) $\mu = 0.92$. The black horizontal line shows the measured interface depth, and the grey shaded region indicates the variation in the measurement. The green horizontal line shows the interface depth predicted by the volume balance model.

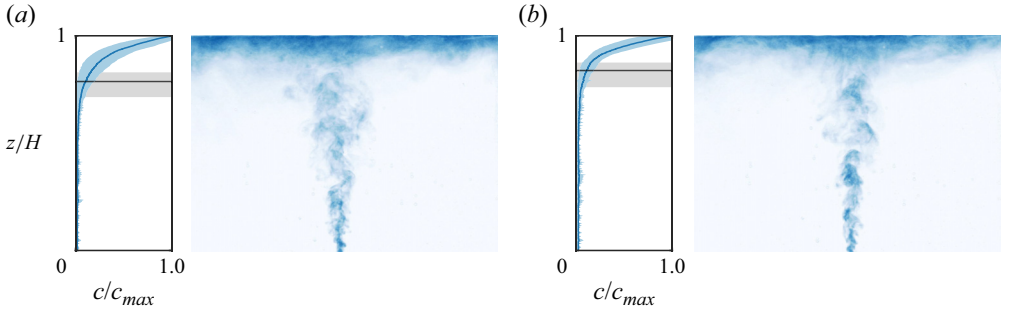

Figure 5. Typical experimental results in the over-ventilated regime showing the horizontally averaged dye concentration of five experiments and a false colour image showing the instantaneous dye distribution in the tank for (*a*) $\mu = 0.57$ and (*b*) $\mu = 0.34$. The black horizontal line shows the measured interface depth, and the grey shaded region indicates the variation in the measurement.

Furthermore, within the under-ventilated regime, the measured depth (black lines) is significantly lower than the prediction using the volume balance (green lines).

Between the experiments, there are differences in the detailed structure of the vertical stratification. In figure 3(*a*), showing an under-ventilated steady state, there is little variation in the concentration outside of a narrow adjustment zone between layers. However, as μ decreases, the adjustment zone expands, and a gradient develops close to the ceiling, producing a kink in the profile. This can be seen in figures 4(*a*) and 4(*b*). In figure 5(*b*), the system is significantly over-ventilated, and the concentration continually adjusts over the full depth of the upper layer. These changes to the mean profile are also accompanied by larger concentration fluctuations as μ decreased.

Generally, there was increased fluid motion close to the interface as μ decreased. For example, at large μ, there were only some small, low-frequency oscillations close to where the plume crossed into the upper layer. As a result, there was little variation in the measured interface depth in figures 3(*a*) and 3(*b*). Close to critical ventilation, we observed rapid, small-amplitude oscillations over the entire surface area of the interface. This resulted in a larger variation in the measured depth of the interface in figures 4(*a*) and 4(*b*). Finally, in the over-ventilated regime, we observed large-scale fluid motion resulting in significant variation in the measured interface depth in figures 5(*a*) and 5(*b*). This behaviour appears

to be correlated with the intermittent arrival of eddies in the plume, and a zone of strong mixing close to where the plume impacts the upper boundary. In the case of a small inner tank, the laterally spreading eddies may reach the side walls and reflect. By repeating the experiments in tanks of different cross-sectional area, we show, later in the paper, that any secondary mixing produced by this overturning is less significant than the central mixing zone.

Based on these observations, we infer that there is an additional flux of fluid from the lower layer mixed into the upper layer to balance the ventilation volume flux. We propose that this results from the turbulent mixing as the plume reaches the upper boundary and spreads laterally, which is associated with the kinetic energy flux supplied by the plume. This leads to entrainment of fluid from the lower layer into the upper layer, which then mixes with fluid supplied by the plume. In the under-ventilated regime, the interface is low, so the plume supplies relatively little kinetic energy. As a result, there is minimal entrainment. In the over-ventilated regime, the interface is higher, so the plume supplies more kinetic energy; furthermore, with the same source of buoyancy, the density contrast is reduced. Both of these factors facilitate the mixing.

3. The model

To model the steady flow, we consider a turbulent plume that develops from a maintained localised source of buoyancy flux πF_0 in a room of total height H and uniform cross-sectional area πA. Letting z denote the vertical distance above the floor, the buoyancy source is at $z = 0$, and the upper and lower vents are at $z = H$ and $z = 0$, respectively. The ventilation volume flux is πQ_V, and incoming air has density ρ_a. At a steady state, the depth of the lower layer is h. This is shown schematically in figure 1.

3.1. *Plume theory*

The theory of turbulent buoyant plumes builds on the seminal work of Morton *et al.* (1956) and is discussed in detail elsewhere, (e.g. List 1982; Linden 2003; Woods 2010; Hunt & Van Den Bremer 2011). In an unstratified environment, the specific volume πQ_p, momentum πM and buoyancy πF fluxes in a plume are

$$Q_p(z) = \lambda F_0^{1/3}(z + z_0)^{5/3}, \quad M(z) = \left(\frac{9\alpha}{10}\right)^{2/3} F_0^{2/3}(z + z_0)^{4/3}, \quad F(z) = F_0, \quad (3.1a\text{–}c)$$

where $\alpha = 0.127$ is the entrainment coefficient (Morton *et al.* 1956) and we have defined the related constant $\lambda = (6\alpha/5)(9\alpha/10)^{1/3}$ for convenience in our solutions. The value of α was determined from a series of separate filling box experiments using our experimental apparatus and is within the range of existing experimental and numerical data for plumes. Here, z_0 is the distance of the virtual origin behind the source. This is the location where a pure source of buoyancy flux πF_0, with zero volume flux and zero specific momentum flux, would produce an identical flow in the far field after a zone of flow establishment close to the source. These solutions assume that the plume is unconfined. Still, they apply to a confined plume if it occupies a small fraction of the total cross-sectional area (Baines & Turner 1969). This requires that

$$\frac{H^2}{A} \ll \left(\frac{5}{6\alpha}\right)^2. \quad (3.2)$$

As seen in table 1, this is true for all our experiments. The distance of the virtual origin behind the actual source, z_0, scales with the source radius but also depends on

Series	$Q_v/\mathrm{cm}^3\ \mathrm{s}^{-1}$	$F_0/\mathrm{cm}^4\ \mathrm{s}^{-3}$	$Q_0/\mathrm{cm}^3\ \mathrm{s}^{-1}$	z_0/cm	H/cm	H^2/A	μ	Symbol
1	4.8–51.5	27.5	0.385	1.4	30.1	4.55	1.30–13.78	○
2	4.8–51.5	41.8	0.385	1.2	30.0	4.52	1.48–15.76	◇
3	5.0–51.8	8.11	0.385	1.7	16.9	1.44	0.34–3.40	□
4	21.5	40.4	0.373	1.2	12.2–36.7	0.75–6.77	0.79–4.93	△
5	13.0–50.7	40.1	0.371	1.2	18.7	0.18	0.68–2.66	∗
6	18.5–49.3	13.0	0.371	1.5	19.0	1.54	0.49–1.32	×

Table 1. Experimental conditions for the experiment series presented in figure 6. In each series, the area of the tank was fixed while the ventilation rate (series 1–3, 5 and 6) or height (series 4) was adjusted to vary μ. These were adjusted in equal steps between the minimum and maximum values presented in the table. The values for H include the virtual origin correction.

the dimensionless source parameter, Γ, given by

$$\Gamma = \frac{5Q_0^2F_0}{4\alpha M_0^{5/2}}. \tag{3.3}$$

In our experiments, Γ is of order one, indicating that the source is close to a pure plume balance. So, approximately

$$z_0 = \lambda^{-3/5}Q_0^{3/5}F_0^{-1/5}. \tag{3.4}$$

In our experiments, this leads to a virtual origin correction of the order $z_0 \sim 0.01$ m.

3.2. *Energy balance*

The kinetic energy flux, $\pi\dot{E}_K$, associated with the mean upward flow in a plume at a distance z from the origin, is

$$\dot{E}_K(z) = 2\rho_0\int_0^\infty r\frac{w^3(r)}{2}\,\mathrm{d}r. \tag{3.5}$$

We model the velocity distribution across the plume using a Gaussian profile of the form

$$w(r) = w_G\exp\left(-\frac{r^2}{b_G^2}\right), \tag{3.6}$$

where $w_G(z) = 2M/Q$ is the centreline velocity and $b_G(z) = Q/\sqrt{2M}$ is the effective plume radius. Then (3.5) can be evaluated at the depth of the interface, leading to

$$\dot{E}_K = \tfrac{1}{6}\rho_0 b_G^2 w_G^3 = \tfrac{1}{2}\rho_0 F_0 h. \tag{3.7}$$

From dimensional arguments, we expect that the turbulent kinetic energy flux scales with the kinetic energy flux of the mean flow. However, this contribution is small, typically less than 7 % of that of the mean flow (Cardoso & Woods 1993). Therefore, for simplicity, we assume that the total kinetic energy flux supplied to the upper layer is given by (3.7).

Next, we calculate the rate of work done to entrain fluid from the lower layer into the upper layer. At this stage, we do not restrict the system to a particular mechanism for turbulent entrainment. Rather, we consider a general entrainment flux, Q_e. From the

conservation of volume over the upper layer, the volume flux in the plume plus the rate of turbulent entrainment into the upper layer balances the ventilation volume flux so that the mean interface depth is constant. Therefore, when there is no short circuiting of the flow, the rate of turbulent entrainment is given by

$$Q_e = Q_V - \lambda F_0^{1/3} h^{5/3}. \tag{3.8}$$

This fluid is transported through the upper layer and extracted by the ventilation, with the work involved in the process being

$$\dot{W} = \rho_0 Q_e \int_h^H g'(z)\,\mathrm{d}z. \tag{3.9}$$

As described in § 2.2, the buoyancy of fluid in the lower layer is zero, but the upper layer has a buoyancy profile $g'(z)$ that depends on the ventilation regime. From the conservation of buoyancy over the upper layer, the buoyancy of fluid extracted by the ventilation is $g' = F_0/Q_V$. So, introducing a change of variables

$$\zeta = \frac{z-h}{H-h} \quad \text{and} \quad \hat{g}' = \frac{g' Q_V}{F_0}, \tag{3.10a,b}$$

we can rewrite equation (3.9) as

$$\dot{W} = \rho_0 F_0 (H-h)\left(1 - \frac{\lambda F_0^{1/3} h^{5/3}}{Q_V}\right)\int_0^1 \hat{g}'(\zeta)\,\mathrm{d}\zeta. \tag{3.11}$$

To complete the model, we need a final relation which constrains the rate of mixing across the interface. In § 2, we observed three important turbulent mixing processes in the upper layer: a mixing zone surrounding the plume where it hits the interface or ceiling, eddies in the radial flow which spreads across the ceiling and any overturning at the edge of the box. In the present experiments, visual observations suggest the mixing near the ceiling and then the eddies in the radial flow seem to dominate: the mixing leads to a stratified region above the lower layer. There are different approaches for quantifying such turbulent mixing (cf. Turner 1986). In the present work, we explore the hypothesis that the total rate of work done by this turbulent mixing is proportional to the rate of input of kinetic energy by the plume, and in the next section, we compare the predictions of this model with our new experimental data. By combining equations (3.7) and (3.11), we then obtain

$$\phi \frac{h}{H-h} = 1 - \frac{\lambda F_0^{1/3} H^{5/3}}{Q_V}\left(\frac{h}{H}\right)^{5/3}, \tag{3.12}$$

where ϕ is a parameter that quantifies the fraction of kinetic energy used for entrainment and accounts for the dimensionless shape factor associated with the vertical stratification in the upper layer. Scaling the interface depth, h, by the height of the room, H, and identifying the parameter μ, we can write

$$\phi \frac{\xi}{1-\xi} = 1 - \mu \xi^{5/3}. \tag{3.13}$$

This model suggests that the interface, ξ, is independent of the cross-sectional area and increases monotonically as μ decreases, eventually saturating to a fraction of the total

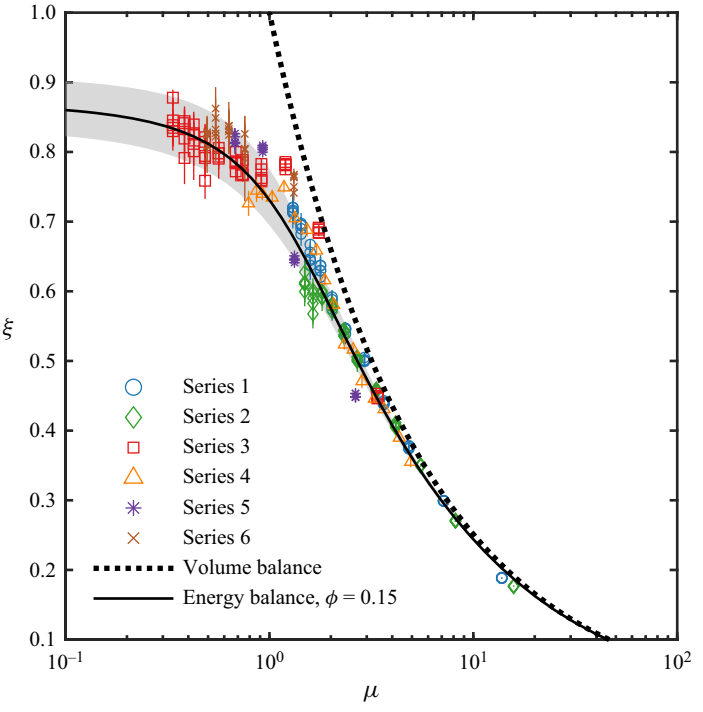

Figure 6. A comparison of measured interface depths (symbols) and theoretical predictions of the volume balance model (dotted line) and energy balance model with $\phi = 0.15 \pm 0.05$ (solid line and shaded region).

room height for very over-ventilated systems ($\mu \to 0$)

$$\xi_0 = \frac{1}{1+\phi_0}. \tag{3.14}$$

Otherwise, in the limit of very weak ventilation, (3.13) approaches

$$\xi = \mu^{-3/5}. \tag{3.15}$$

Thus recovering the expression for the interface depth derived in § 1 using the volume balance model.

4. Comparison of model and experiment

Experiments were performed to compare the measured interface heights with the prediction of the energy balance model developed in § 3. These experiments were conducted with different room heights, cross-sectional areas, source buoyancy fluxes and ventilation rates, as listed in table 1, to establish steady states in the range $0.34 \leq \mu \leq 15.76$.

The distance of the interface from the virtual origin was obtained for each experiment, rescaled by the distance to the base of the model room and is plotted as a function of μ in figure 6. The six series of experiments are consistent and, within the accuracy of the experimental measurements, collapse onto a single curve. Given the large range of tank aspect ratios, $0.18 < H^2/A < 6.77$, this is strong support for the model prediction that the interface depth is independent of the cross-sectional area.

We compare these measured interface depths with the theoretical predictions using the volume balance (dotted line) and the new energy balance model (solid line). The scatter in the experiments suggests that there may be some variation in ϕ but that it only appears to be a very weak function of the experimental conditions. As such, we assume that ϕ is constant across our experiments, and comparison with the data suggests that the optimal fit is obtained by setting $\phi = 0.15$. The sensitivity of our model to the numerical value of ϕ is indicated by the grey-shaded region, which shows the range of predicted interface heights bounded by $\phi = 0.10$ and $\phi = 0.20$. This suggests that our hypothesis that a fraction of kinetic energy is converted to potential energy through mixing is not inconsistent with the data.

The turbulent intensity of mixed fluid in the upper layer is related to the turbulent intensity of the fluid supplied by the plume; this suggests that ϕ may be related to α. However, the process of mixing at the edge of the vertically rising plume is different from the mixing produced as the eddies spread radially from the plume through the upper layer and entrain lower layer fluid. As a result, we have measured the constant ϕ independently of α, but it is nevertheless notable that their values are similar.

Using the value $\phi = 0.15 \pm 0.05$, there is reasonable agreement between the predictions of the energy balance model and the experiments over the full range of experimental conditions and, critically, we can predict the interface depth within the over-ventilated regime. The new energy balance model is also more accurate than the simple volume balance model close to critical ventilation, $1 < \mu \lesssim 2$. However, given the variability between experiments, both models are indistinguishable for significantly under-ventilated systems. This is consistent with our experimental observations in § 2.2, which suggest that turbulent entrainment becomes increasingly significant as μ decreases. To explore this further, we use (3.1*a–c*) and (3.8) to calculate the volume flux in the plume and the volume flux due to entrainment at each interface height. The individual contributions are plotted in figure 7. When the interface is low, the entrainment flux is small, and it is reasonable to assume that the only interfacial transport is in the plume, as in the volume balance model. However, the entrainment flux grows rapidly as ξ increases beyond ≈ 0.5. The shaded region in figure 7 indicates the range of interface depths in our experiments, where entrainment contributed as much as two thirds of the total volume flux into the upper layer.

The energy balance model predicts that the interface depth increases monotonically as μ decreases, reaching a maximum as $\mu \to 0$. Evaluating equation (3.14) for $\phi = 0.15$ leads to $\xi_0 = 0.87$. It is interesting to compare this with the results of Kaye & Hunt (2007), who investigated the initial transient outflow from a plume impinging on the base of a box before it developed a stratification. This initial transient is closely related to a very over-ventilated system where the outflow from the plume is immediately ventilated and does not recirculate in the upper layer. In their experiments, Kaye & Hunt (2007) found that the depth of the fully developed gravity current from the plume was $0.12H$. In the context of this work, this corresponds to $\xi_0 = 0.88$, which is in accord with figure 6 as $\mu \to 0$.

5. Application to natural ventilation

Although it was not the intention of this study, it is interesting to extend the principles of this work to natural ventilation flows where, by analogy to the present work, turbulent mixing in the upper layer may also cause the interface to descend. In natural ventilation, the ventilation volume flux depends on the buoyancy and depth of the upper layer. Since entrainment across the interface will modify the stratification, a full understanding of this process would require new experiments. However, we can directly apply our results

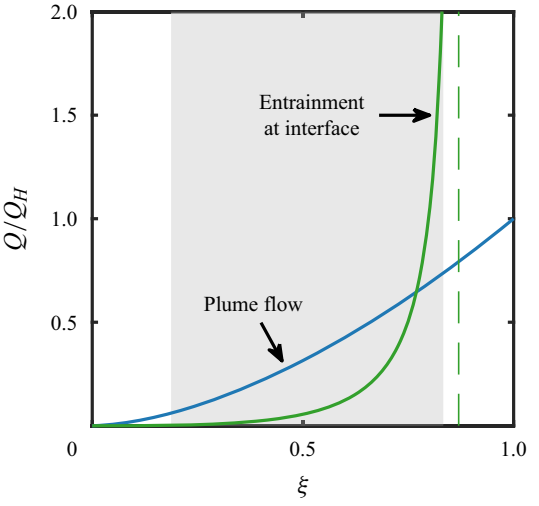

Figure 7. The contribution of turbulent entrainment. Flux into the upper layer from the plume (blue) and flux due to entrainment across the interface (green), depending on the interface height.

to natural ventilation to include the effect of mixing but not a subsequent readjustment. This should give a lower bound for the interface depth, while the original volume balance (Linden *et al.* 1990) provides an upper bound. In a naturally ventilated room, this upper bound is

$$\frac{A^*}{\lambda^{3/2}H^2} = \left(\frac{\xi^5}{1-\xi}\right)^{1/2}, \tag{5.1}$$

where A^* is an effective area of the openings to the surroundings. If there is no mixing, then the only interfacial transport is in the plume, and this volume flux is exactly balanced by the volume flux leaving through the vents, and, in principle, an identical steady state could be reached in a mechanically ventilated system through careful selection of the ventilation rate. Therefore the effective area of the openings, A^*, can be mapped onto an equivalent μ using (1.4) and (5.1). This equivalent μ can be used in (3.13) to estimate the interface depth, including the effect of turbulent mixing, but not the subsequent readjustment. In figure 8, we present experimental data from Linden *et al.* (1990) and Kaye & Hunt (2004) and compare them with the predicted interface depth using (5.1) and our energy balance to account for turbulent mixing. Most of the experimental data lie below the volume model but above our energy balance, suggesting that the two lines are bounds and that a similar turbulent mixing process happens in natural ventilation. Again, turbulent mixing appears to be more important when the interface is higher. It would be interesting to investigate this further and include the effect of changing the vertical stratification.

6. Application to building engineering

One important application of this modelling is predicting the interface depth in a range of building types, where, ideally, the interface between the layers is located above the occupied zone. It is interesting to calculate the value of μ associated with heat sources of different strengths for various ventilation rates to determine the possible ventilation regime and the importance of turbulent mixing. In building engineering, the strength of mechanical ventilation can vary significantly and is typically described in terms of the air

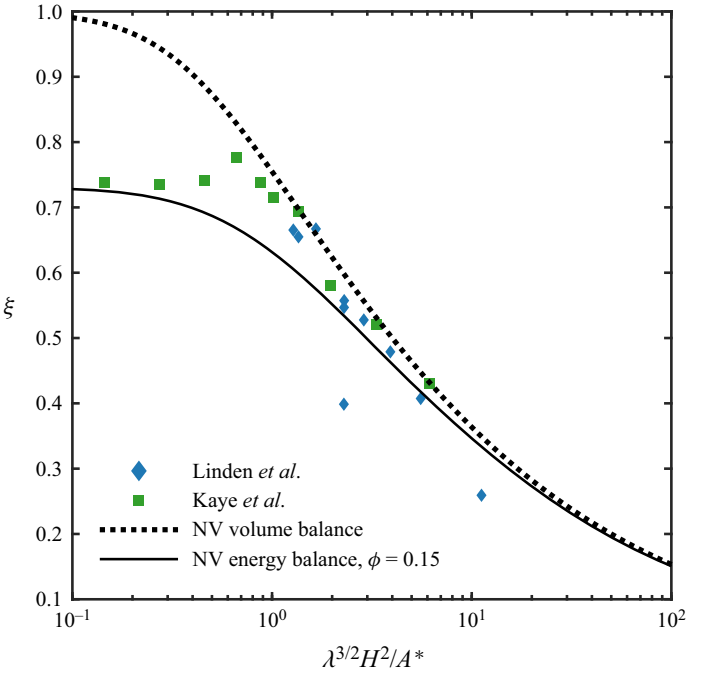

Figure 8. A comparison of measured interface depths (symbols) and theoretical predictions of the volume balance model (dotted line) and energy balance model with $\phi = 0.15$ (solid line) for natural ventilation.

changes per hour (ACH), which is related to the ventilation volume flux, πQ_V, and the volume of the room, $\pi V = \pi AH$, by

$$\mathrm{ACH} = 3600\frac{Q_V}{V}. \tag{6.1}$$

6.1. *A single localised heat source*

To examine the importance of mixing, we first consider the idealised limiting case in which the total heat load originates from a small area, forming a single plume in the far field. For a thermal plume rising above a heat source with heat load Θ, the buoyancy flux is

$$\pi F_0 = g\frac{\beta\Theta}{\rho_0 C_p}, \tag{6.2}$$

where β is the thermal expansion coefficient and C_p is the specific heat capacity of air. Individual heat sources can range in strength from $\Theta = 0.1$ kW for the human thermal plume to $\Theta = 1$–3 kW for large electrical equipment or dedicated heating appliances. Stronger heat sources are also possible, often generated through indoor combustion or as the combined effect of multiple closely placed heat sources.

In figure 9, we show the value of μ as a function of the heat load for a localised heat source with strength in the range 0–5 kW for a room of width 6 m and height 3 m above the virtual origin of the heat source. As discussed in § 4, we suggest that turbulent entrainment across the interface is significant for $\mu \lesssim 2$, and the ventilation may be modelled using the energy balance model we have proposed. Even at lower ventilation rates, for example, 6 ACH, which is typical for an office, the cross-over heat load occurs at $\Theta = 1.6$ kW.

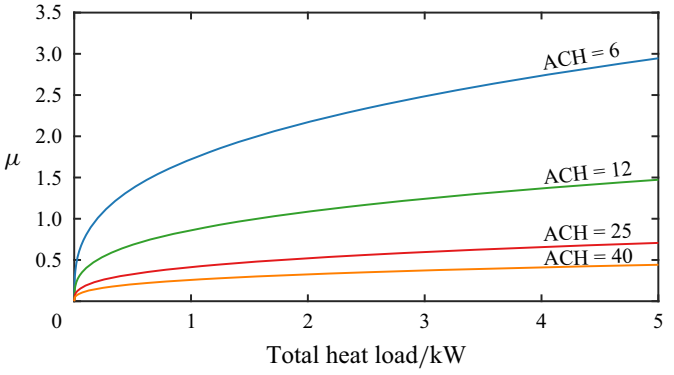

Figure 9. The value of μ for a range of heat loads in a mechanically ventilated operating theatre for 6, 12, 25 and 40 ACH.

As a result, it may be important to account for turbulent mixing in spaces with small to moderate heat loads. Only spaces with large heat loads can neglect entrainment into the upper layer when designing the ventilation.

6.2. *Multiple distinct heat sources*

Often, the total heat load in a building is spread between many distinct heat sources, and extending the model to examine this situation in comparison with a single heat source is of interest. For simplicity, we restrict our attention to n heat sources of equal strength. This may approximate an office space with multiple occupants where each person generates a similar heat load.

To model this situation, we assume that the mixing associated with each plume is independent, as applies to a small number of heat sources placed far apart. However, we note that if the spacing between the sources is not sufficient, the mixing across the interface in the upper layer associated with the different heat sources will likely interact, leading to a more complex process. With n independent heat sources of buoyancy flux F_0/n, (3.12) is replaced with the relation

$$\phi\frac{h}{H-h} = 1 - \frac{n^{2/3}\lambda F_0^{1/3}H^{5/3}}{Q_V}\left(\frac{h}{H}\right)^{5/3}, \tag{6.3}$$

which depends on the modified dimensionless parameter

$$\mu_n = \frac{n^{2/3}\lambda F_0^{1/3}H^{5/3}}{Q_V}. \tag{6.4}$$

We see that $\mu_{n+1} > \mu_n$, suggesting that distributing the same total heat load over a larger number of heat sources causes the interface to descend. Using (6.4), the depth of this interface is equal to the depth produced by a single heat source with a heat load which is n^2 times larger, although in that case, the buoyancy of the upper layer is different. As a result, the space is more likely to be under-ventilated than with a single heat source.

Linden *et al.* (1990) examined a similar situation in natural ventilation. They showed that spreading a heat load between n distinct heat sources results in the same interface depth as a single heat source where the effective area of the openings has been decreased by a factor of n. This causes the interface to descend, but unlike the present case, the new depth does not depend on the strength of the heat source, only the number.

The modified parameter, μ_n, has an important effect on the value of the critical cross-over heat load, which is reduced by a factor of n^2. For example, in the 6 ACH case, the cross-over heat load is reduced to $\Theta = 0.4$ kW when there are two equal heat sources and to $\Theta = 0.18$ kW when there are three. Therefore, increasing the occupancy from two to three people may cause the ventilation flow to transition from a regime where it is important to consider turbulent mixing to one where it may be appropriate to neglect this effect. At moderate ventilation rates, such as 12 ACH, the cross-over heat load for a single source is very large, $\Theta = 13$ kW. However, with multiple heat sources, this reduces to 3.3 kW and 1.4 kW if the heat supply is distributed between two or three heat sources, respectively, which are more typical of the expected heat loads in the built environment. Currently, many hospital operating theatres have ventilation rates of 20–25 ACH, and some have ventilation rates over 40 ACH. These large ventilation rates mean the operating theatre is over-ventilated even for very large heat loads spread across multiple heat sources. Therefore, it is almost always important to account for turbulent mixing in determining the stratification at the top of the space.

7. Conclusions

We have explored the interaction of natural convection and mechanical ventilation in a room where fresh air is supplied at low level and stale air is extracted at high level. Turbulent buoyant plumes from heat sources interact with this upward airflow and establish a two-layer stratification. This work complements previous studies on natural ventilation by extending the concepts to mechanical ventilation, which is more widespread.

A key and novel observation from our experiments is the identification that an over-ventilated regime develops in which the volume flux in the plume is less than the ventilation volume flux. In this case, a simple volume balance model in which the upward flow is assumed to be given by the sum of the plume flow and the remaining ventilation flow leads to the prediction that the space is filled with the cold supply air. However, our new experiments show that the system retains a two-layer stratification. Our observations suggested that turbulent mixing in the upper layer associated with the kinetic energy flux supplied by the plume entrains fluid from the lower layer into the upper layer.

We propose a new model which is able to predict the interface depth based on an energy balance between the kinetic energy flux supplied by the plume and the rate of work done to entrain fluid from the lower layer into the upper layer. We find that this model leads to predictions which are consistent with the interface height measured in our experiments across both regimes. Finally, we show that it is important to consider this turbulent mixing when designing ventilation systems, particularly for operating theatres or other rooms with a large ventilation rate.

Declaration of interest. The authors report no conflict of interest.

Author ORCIDs.
Daniel A. Toy https://orcid.org/0009-0008-8031-411X;
Andrew W. Woods https://orcid.org/0000-0002-5098-9940.

Appendix A. Identification of the interface

In studies on natural ventilation, the layer interface has sometimes been defined by the location of the largest gradient in light intensity (Kaye & Hunt 2004). However, when turbulent entrainment is significant, gradients in light intensity may develop over a large part of the upper layer, leading to significant uncertainty in the location of the interface.

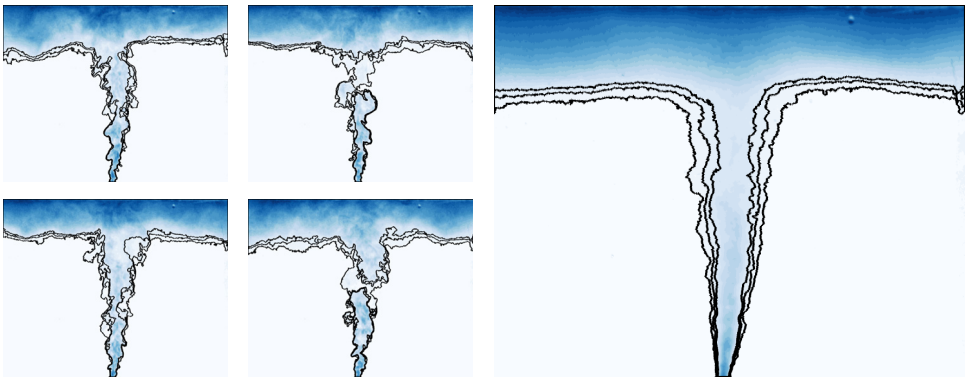

Figure 10. Experimental results for $\mu = 0.6$, annotated to show the 5 %, 10 % and 15 % contours. The left-hand panels show an instantaneous snapshot of the steady state, and the right-hand panel shows the time-averaged distribution.

This is why, in the study of plumes and gravity currents, a cutoff light intensity is typically used to define the flow boundary (Morton *et al.* 1956; Hacker, Linden & Dalziel 1996). In this study, we follow this approach and define the interface by the average height of the contour, where the light attenuation is 10 % of the maximum.

The left-hand panels in figure 10 show four snapshots of a steady state for $\mu = 0.6$ taken 60 s apart and have been annotated with the 10 % contour. The 5 % and 15 % contours are also shown to indicate the uncertainty in the measurement. Between the panels, there is some variation in the location of the contours due to fluid movement at the interface. Therefore, to ensure consistency, the total amount of dye inside the 10 % contour, which should be constant, was calculated at successive times for each experiment. This amount was constant within 5 % for $\mu \gtrsim 0.5$, and within 10 % for $\mu \lesssim 0.5$.

To calculate the average position of the interface, we produce a time average image before locating the 10 % contour. This is shown in the right-hand panel in figure 10. To calculate the final estimate for the interface depth, we take an average of the height of the 10 % contour, excluding the plume region.

Appendix B. Short circuiting of the flow

When performing any mechanical ventilation experiments, there is a possibility for short circuiting of the flow: in the context of the experimental system shown in figure 2, this would result in a disturbance to the interface so that fresh water is drawn directly into the outlet pipe without mixing with the salty layer. Hassan, McKeon & James (2022) investigated this phenomenon and found that for a given extraction flow, q, the transition to short circuiting occurs when the distance from the opening in the outflow pipe to the density interface, S, has a value smaller than a critical value S_c, where

$$S_c = 0.69 \left(\frac{q^2}{\Delta g'} \right)^{1/5}, \tag{B1}$$

with $\Delta g'$ being the buoyancy contrast across the interface.

Equation (B1) suggests that short circuiting is more likely to become significant when the fluid is withdrawn unevenly from the space, with a relatively large outflow in one location. Therefore, our experiments are designed with up to eight well-spaced outlet pipes, and in almost all of our experiments, we estimate that $S > S_c$ so there is no short

circuiting. However, in two particular experiments from series 3, with $\mu = 0.34$ and 0.54, we estimate that $S_c > S > 0.9S_c$.

To investigate the potential impact of short circuiting on these experiments, we carried out an additional series of experiments (series 6) in a modified experiment set-up where an acrylic plate with dimensions 0.20 by 0.20 m was placed horizontally as a false floor, 0.1 m above the base of the tank. This apparatus formed a mixed layer above the acrylic plate, and a low-velocity outflow developed through the gap, of width 2.5 cm, between the tank's walls and the edge of the plate. This slow flow caused minimal disturbance to the stratified layer above the plate.

Using this modified apparatus, we find that, within experimental error, the depth of the mixed layer is identical to the experiments from series 3, suggesting that short circuiting was negligible in these experiments. More generally, for each value of μ, the experiments in series 6 were consistent with those using the outflow pipes.

References

Baines, W.D. & Turner, J.S. 1969 Turbulent buoyant convection from a source in a confined region. *J. Fluid Mech.* **37** (1), 51–80.

Cardoso, S.S. & Woods, A.W. 1993 Mixing by a turbulent plume in a confined stratified region. *J. Fluid Mech.* **250**, 277–305.

Hacker, J., Linden, P.F. & Dalziel, S.B. 1996 Mixing in lock-release gravity currents. *Dyn. Atmos. Oceans* **24** (1–4), 183–195.

Hassan, S., McKeon, C.D. & James, D. 2022 Predicting transition from selective withdrawal to entrainment in two-fluid stratified systems. *Phys. Rev.* E **105** (5), 055109.

Hunt, G.R. & Van Den Bremer, T.S. 2011 Classical plume theory: 1937–2010 and beyond. *IMA J. Appl. Maths* **76** (3), 424–448.

Kaye, N.B. & Hunt, G.R. 2004 Time-dependent flows in an emptying filling box. *J. Fluid Mech.* **520**, 135–156.

Kaye, N.B. & Hunt, G.R. 2007 Overturning in a filling box. *J. Fluid Mech.* **576**, 297–323.

Linden, P.F. 2003 *Convection in the Environment*, illustrated edn. Cambridge University Press.

Linden, P.F., Lane-Serff, G.F. & Smeed, D.A. 1990 Emptying filling boxes: the fluid mechanics of natural ventilation. *J. Fluid Mech.* **212**, 309–335.

List, E.J. 1982 Turbulent jets and plumes. *Annu. Rev. Fluid Mech.* **14** (1), 189–212.

Morton, B., Taylor, G. & Turner, J. 1956 Turbulent gravitational convection from maintained and instantaneous sources. *Proc. R. Soc. Lond.* **234** (1196), 1–23.

Turner, J.S. 1986 Turbulent entrainment: the development of the entrainment assumption, and its application to geophysical flows. *J. Fluid Mech.* **173**, 431–471.

Woods, A.W. 2010 Turbulent plumes in nature. *Annu. Rev. Fluid Mech.* **42**, 391–412.